Ancient TL

www.ancienttl.org · ISSN: 2693-0935

Martin, L., Incerti, S. and Mercier, N., 2015. *Comparison of DosiVox simulation results with tabulated data and standard calculations.* Ancient TL 33(2): 1-9.
https://doi.org/10.26034/la.atl.2015.493

Ancient TL

# Comparison of *DosiVox* simulation results with tabulated data and standard calculations

Loïc Martin[1,*], Sébastien Incerti[2,3], Norbert Mercier[1]

[1]Institut de Recherche sur les Archéomatériaux, UMR 5060 CNRS - Université Bordeaux Montaigne
Centre de Recherche en Physique Appliquée à l'Archéologie (CRP2A)
Maison de l'archéologie, 33607 Pessac Cedex, France

[2]CNRS, IN2P3, CENBG, UMR 5797, 33170 Gradignan, France
[3]Université de Bordeaux, CENBG, UMR 5797, 33170 Gradignan, France

[*]Corresponding Author: loic.martin@u-bordeaux-montaigne.fr

*Received: August 14, 2015; in final form: November 17, 2015*

## Abstract

**The *DosiVox* software allows modeling various situations of dosimetric interest for trapped charge dating methods. Simulation of $\alpha$-, $\beta$- and $\gamma$-dose rates are considered here in adapted modeling. The results of numerical simulations are compared with tabulated data of dose attenuation in layers and grains usually used in the dating community. Good agreements are found with the tabulated data, and some limits of usual approximations are highlighted.**

**Keywords: *DosiVox*, dose rate modeling, software, Geant 4**

## 1. Introduction

*DosiVox* is a Geant4 based software for simulating dose rates in various contexts encountered in trapped charge dating methods. It is freely available[1] and has already been used in two studies: in the first one (Martin et al., 2015a) its features were illustrated by a series of selected examples, while in the second, Martin et al. (2015b) presented dose rate modeling of a complex sediment sample previously characterized by numerous analytical techniques. Meanwhile, considering the diversity of samples and dosimetric contexts that can be encountered in trapped charge dating and for which numerical simulations can be of interest to assess the effect of distinct parameters on the dose rates, it is difficult to evaluate the reliability of the modeling results because of the lack of comparative data. We propose in this paper to test *DosiVox* in dosimetric layouts described in the literature for which tabulated data are available. The relevance of the compared data will be discussed as well as the limits of the usefulness of these modelings.

[1] http://www.iramat-crp2a.cnrs.fr/spip/spip.php?article144

## 2. Procedure

The *DosiVox* software allows modeling samples by constructing a voxelised (3D) volume where the material and the associated radioactivity can be defined in each voxel. The emission of $\alpha$-, $\beta$- and $\gamma$-particles from the natural radioactive elements can be simulated and the corresponding dose rates can be recorded by different detector types (Martin et al., 2015a). The software does not need any programming skills, all the parameters used to construct the simulation being defined with a "pilot" text file. For the purpose of this study, *DosiVox* version 1.03 was used. A new feature of particle reflection on the walls of the volume, not yet available in the online version of the software, was sometimes used in the simulations in order to speed them up and to increase the statistical counting. However, all the results reported here were first tested without this option, to ensure that it has no effect on the exactness of the results.

We propose to arrange this study in three parts, each of them considering a particular *DosiVox* detector type with its own utility and purpose. The simulations, results and discussions of each case are presented in the corresponding part for

a better consistency.

In the first part, the dose rate profiles generated by a juxtaposition of layers differing by their radioactivity are investigated. The results concerning the $\gamma$-dose rates are compared to the data gathered by Aitken (1985). Simulations of the $\beta$-dose attenuation in a silica layer of variable thickness have been carried out in a similar way as Brennan (2006)'s calculations. At last, the attenuation of the $\alpha$-dose rate in calcite layers calculated by *DosiVox* is compared to the data from Grün (1987). All these dose rates were recorded with the "Probe" detector of *DosiVox*, a detector composed of a cylinder crossing through the height of the modeled volume and divided in several parts, each one recording the dose deposits.

The second part explores the modeling of dose attenuation effects in sedimentary grains, using the grain packing detectors of *DosiVox*. These detectors were mainly set in an almost infinite matrix layout because the majority of the available data had been calculated for this situation. Both internal and external dose deposits were calculated for 100 $\mu$m grains using $\alpha$- and $\beta$-radiations, and for 1 mm grains as well in the case of the $\beta$-particles. The results are compared to the tabulated data from Bell (1980), Guérin et al. (2012) and Martin et al. (2014). The effect of water content and matrix material are also briefly investigated in the case of the $\beta$-dose rate, for a comparison with Nathan & Mauz (2008) data. In addition, a test to check for the complementarity of the internal and external $\beta$-dose rates is presented for a packing of 400 $\mu$m grains.

The last part of the study focuses on the subvoxelised detector of *DosiVox* that allows detailing an object with a finer level of resolution. Voxelised sphere modelings were used for these tests because several data concerning the attenuation of dose in spherical volumes can be found in the literature, for $\alpha$- (Bell, 1980; Martin et al., 2014) $\beta$- (Mejdahl, 1979; Fain et al., 1999; Guérin et al., 2012) and $\gamma$-radiations (Mejdahl, 1983; Aitken, 1985). The possibilities offered by *DosiVox* for visualizing the dose deposits are used to illustrate the kind of information that simulations can bring for apprehending dose rate distributions.

Some of the simulation results presented in this paper are normalized to the quantity of energy carried by the primary particles emitted by unit of mass (*EmMass*) in the material used as a reference. This value is homogeneous with a dose, and corresponds to the infinite matrix dose of the reference material. Meanwhile, as the main purpose of *DosiVox* is to investigate dose rates in cases which are far away from the infinite matrix case, the *EmMass* term can be considered more adapted to this context. Normalizing the dose results provided by the simulation by the *EmMass* term is a convenient way to proceed because it allows representing them as values relative to a calculable annual dose. This ratio (simulated dose divided by *EmMass*) is therefore proportional to a dose rate as it only requires to be multiplied by the corresponding specific annual dose of the radioelement present in the reference material, taken from Guérin et al. (2012) for instance.

## 3. Layer to layer variation

### 3.1. Variation of dose rate from a radioactive layer to an inert one

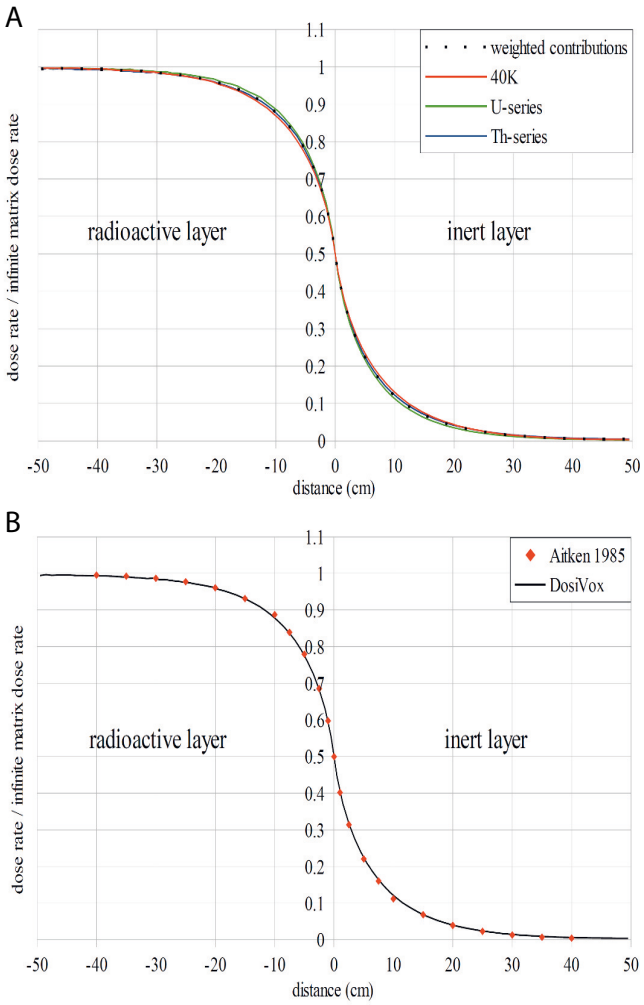


Figure 1. $\gamma$-dose rate in a radioactive layer next to an inert layer.

This first simulation layout is presented in appendix H of Aitken's book (Aitken, 1985). A radioactive layer of soil is next to an inert layer of an identical soil. The $\gamma$ dose rate profile from the $^{40}$K, U- and Th-series spectra are investigated at the interface of the two media. The different spectra are taken from the *DosiVox* data (Martin et al., 2015a), the decay chains of the U- and Th-series being in secular equilibrium. The chemical composition of the soil is taken from Aitken: O 50 %, Si 36 %, Al 6.9 %, Ca 0.5 %, Fe 3.5 %, Mg 0.4 %, K 1.5 %, Na 0.6 %, Ti 0.6 %. The dry soil density is 1.6 g cm$^{-3}$, and the moisture represents 25 % of the dry mass which leads to a total density of 2 g cm$^{-3}$ for the moist sediment. Figure 1 shows the dose rate profiles of the $\gamma$ emissions from the different spectra, and the weighted mean of their contribution for contents of 1 % in mass of K, 3 ppm of U and 10 ppm of Th (which corresponds to weights of 20 % for the $^{40}$K dose rate, 30 % for the U-series and 50 % for the Th-series). These proportions were also used by Aitken (1985).

Aitken's results are represented on Fig. 1 for comparison.

We can observe that the results of the *DosiVox* simulations match very well the data from Aitken (1985). Few difference can be observed and likely result from the evolution of $\gamma$-spectra and cross section values since 1985.

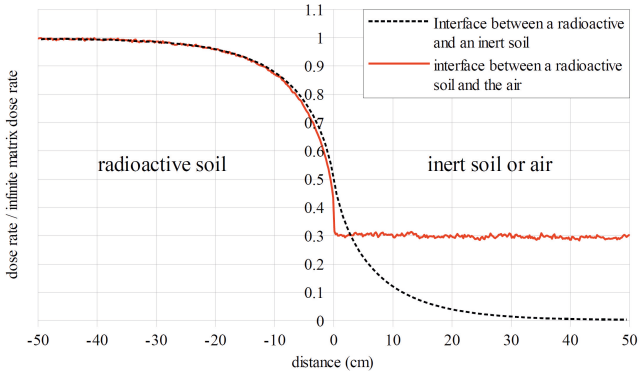


Figure 2. $\gamma$-dose rate next to the surface of a soil.

Aitken estimated that the curve part representing the dose rate in the radioactive layer (from -50 to 0 cm on the horizontal axis) could be used to calculate the dose rate at the surface of a soil, considering that the inert part is replaced by air. However, by replacing the one meter-thick inert soil layer, by an equal volume of air (N 78 %, O 22 %, density = 0.00129 g cm$^{-3}$, water content = 0 %), the *DosiVox* simulation result presented on Fig. 2 indicates a profile significantly different. The lower dose rate observed from -15 cm to 0 cm results from a lack of back-scattered $\gamma$-particles from the meter of air next to the soil, in comparison with the quantity of particles back-scattered by the inert soil in the previous simulation. The assumption of Aitken was yet not wrong because if a length of air superior to the $\gamma$-range in this material had been simulated, the back-scattered $\gamma$-particles in air would have compensated the lower dose rate in the first fifteen centimeters of soil. But in a real case of measurement, this back-scattered $\gamma$-flux is mixed with all the $\gamma$-rays coming from adjacent sediments, as they have a long range in air. Considering the very different ranges of the direct $\gamma$-self-irradiation of the soil and of the back-scattered particles in the air, it could be more pertinent to take in account separately these two contributions to the total $\gamma$-dose rate at the surface of the sediment.

We can observe in Fig. 1A that the Th-series $\gamma$-dose rate profile is very close to the weighted $\gamma$-dose rate profile. Therefore, the Th-series $\gamma$-spectrum will be used for the next simulations of $\gamma$-rays, because it is directly available in *DosiVox* and can be considered as representative of an average behavior of $\gamma$-radiations.

A similar situation is considered now for the $\beta$-dose rate, but we replaced the soil material by pure silica. This layout corresponds to the geometry considered by Brennan et al. (1997) for calculating $\beta$-dose rate attenuation in a silica layer of variable thickness. The silica material is composed of $SiO_2$ 100% with a density of 2.65 g cm$^{-3}$ and no moisture.

The $\beta$-doses deposited in the inert layers for the $^{40}$K, U-series and Th-series spectra are given in Fig. 3. The x-axis represents the thickness of the inert silica layer, and the dose rates are expressed as the percentage of the dose rate in an infinitely thin inert layer next to a radioactive one. These results were obtained by averaging the dose recorded in the segments of the "Probe" detector overlaying the inert part of the model for the considered thickness. The *DosiVox* results are compared with the data calculated by Brennan et al. (1997) using the ROSY software and the Monte-Carlo calculations of Cross et al. (1992), and with the data from Grün (1986) reported by Brennan et al. (1997) in his paper.

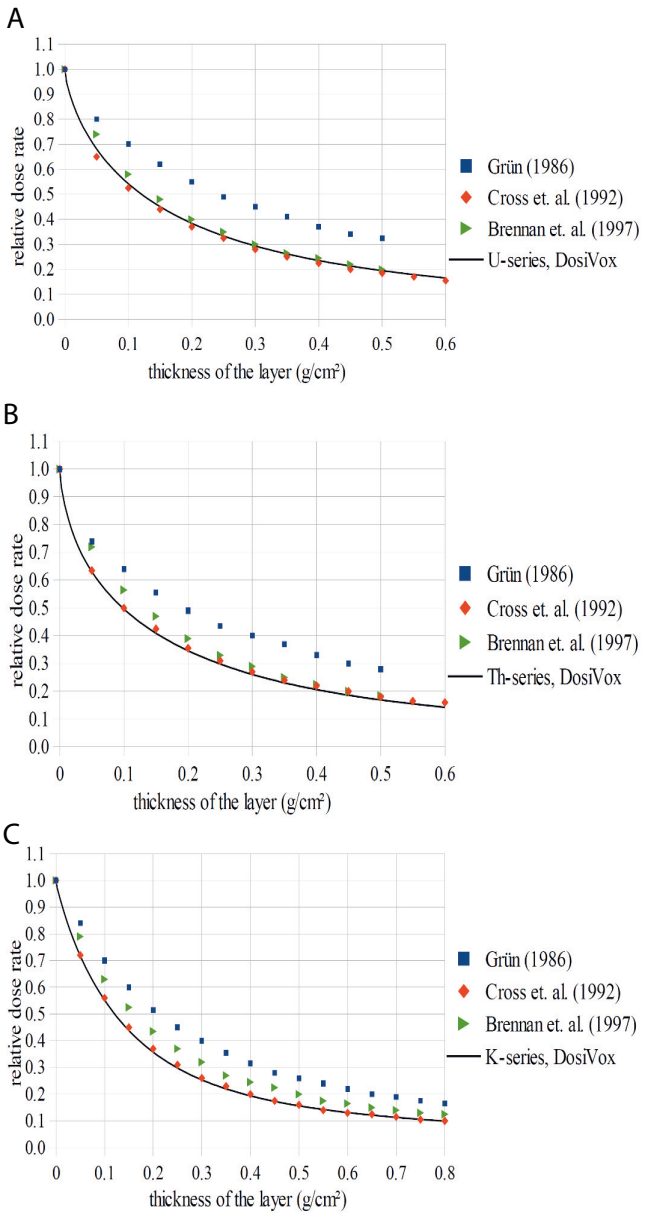


Figure 3. $\beta$-dose rate in a silica inert layer next to a radioactive layer

The *DosiVox* results are consistent with the data obtained by Brennan et al. (1997) by applying the table of Cross et al. (1992) on a silica medium. This agreement makes sense

since as for *DosiVox*, the Cross tables were calculated using Monte-Carlo simulations and Brennan considered the different contributions of the natural $\beta$ emitters.

A similar approach using planar geometries had been carried out by Grün (1987) for calculating the attenuation of $\alpha$-dose rate in mollusc shells: a radioactive sediment next to a layer of calcite (representing the shell) had been studied. We reproduced these calculations using a similar modeling to the one used for the $\gamma$- and $\beta$-dose rate simulations, but in the present case, the radioactive part was filled with a typical dry clay sediment ($SiO_2$ 54 %, $Al_2O_3$ 46 %, density: 1.8 g cm$^{-3}$) and the inert part with pure calcite ($CaCO_3$, density: 2.7 g cm$^{-3}$). As previously, the dose rate in a layer of a particular thickness was calculated by averaging the dose recorded in the corresponding "Probe" segments, and by dividing this number by the *EmMass* value of the sediment. The *DosiVox* results are compared to those of Grün (1987) in Fig. 4. The *DosiVox* dose rates follow the trend of Grün's results, and are in quite good agreement even if they are slightly lower. This small difference could be explained by a difference in the sediment composition or in the equations describing the interaction of $\alpha$-particles with calcite at different energies.

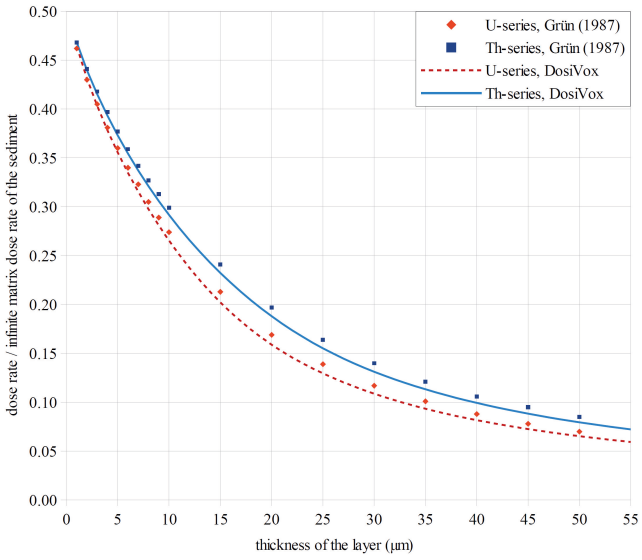


Figure 4. $\alpha$-dose rate in a calcite inert layer next to a radioactive sediment layer.

### 3.2. $\gamma$-dose rate in a radioactive layer between two less radioactive media

We are now considering a little more complex layout of a soil layer sandwiched between two less radioactive media. This case was also presented by Aitken (1985) in the appendix H of his book: the internal layer was two times more radioactive than the surrounding soils. We considered two cases, when the internal layer is 4 cm thick and when it is 40 cm thick. The Th-series $\gamma$-spectrum was used, and the chemical composition, density and moisture of the soils are identical to those of section 1.1. The dose rate profiles were calculated separately for the internal layer and for the twice less radioactive soils, and are presented in Fig. 5. For both thicknesses, the sum of these two contributions are also indicated, as well as the data from Aitken. In the case of a 4 cm thick internal layer, a simulation in one shot of both the radioactivity of the layer and the surrounding soils was also carried out and the results are presented on Fig. 5A.

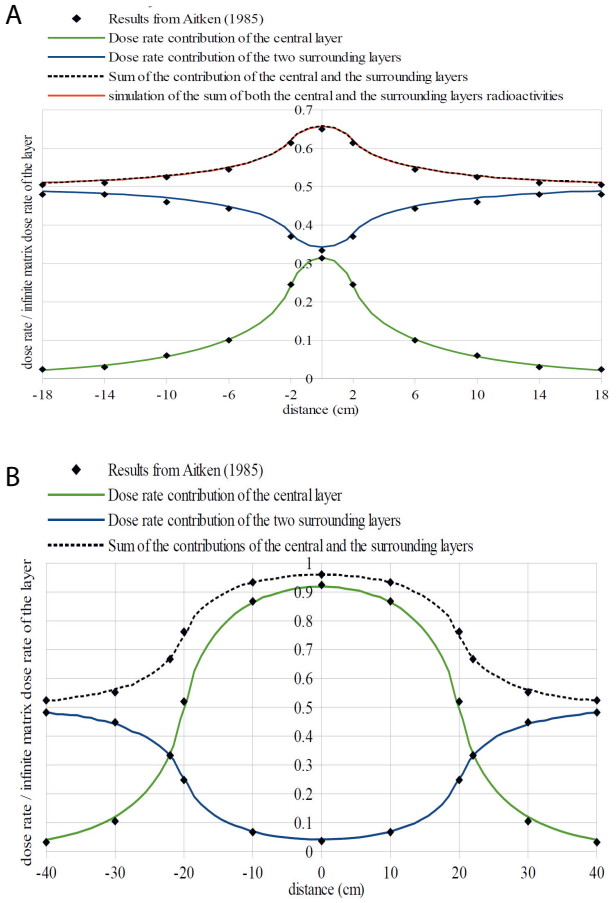


Figure 5. $\gamma$-dose rate in a layer between two soils having half as much radioactivity

As we can see, there is excellent agreement in both cases with the Aitken calculations. In the case of the 4 cm layer, the dose rate from the surrounding layers, and consequently the sum of the dose rates, is just a little bit lower compared to Aitken's data. This effect may be due to the use of the Th-series spectrum instead of a weighted spectrum resulting from a combination of $^{40}$K, U- and Th-series spectra, but the difference is very small. We can also observe in this case that the sum of the dose rate from the two contributions perfectly matches the dose rate profile obtained by simulating in one shot both the radioactivities of the layers and of the two soils, suggesting that these two ways of calculation are consistent with each other. In other words, the principle of superposition of dose rates is conserved by *DosiVox*.

In addition to these dose rate profiles, Aitken (1985) also investigated the variation of the dose rate at the center of the layer, surrounded by non-radioactive levels, with its thick-

ness. The results obtained for various thickness values with *DosiVox* are compared to Aitken's calculations in Fig. 6. These results are also in good agreement: only small differences can be observed, which may be caused by the use of only the Th-series spectrum, or to changes in the nuclear data since Aitken's publication.

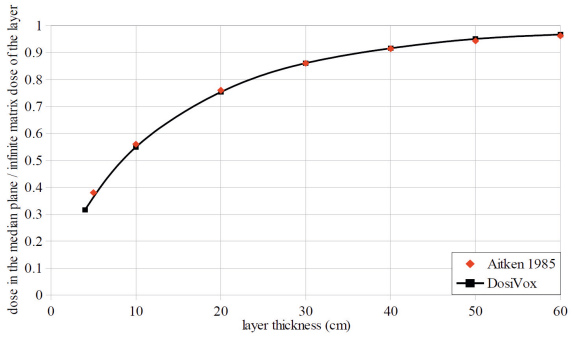


Figure 6. $\gamma$-dose rate in median plane of radioactive layer between two inert regions.

## 4. $\alpha$- and $\beta$-dose rates in spherical grains

The sedimentary grains can be considered as the most frequently dated objects with paleodosimetric methods. We propose in this part to test the reliability of *DosiVox* for representing the dose rate affecting quartz grains in standard cases. Considering that the grain sizes usually used are significantly smaller than the mean range of the $\gamma$-rays (which limits the dosimetric effects that can be induced by the presence of grains), the following simulations are focused on the $\alpha$- and $\beta$-dose rates only.

### 4.1. $\alpha$- and $\beta$-dose rate in infinite matrix conditions

In most cases, a sedimentary grain is considered as a small heterogeneity in a uniform and infinite matrix. According to this model, the dose received by a grain depends on the infinite matrix dose rate (which is replaced by the *EmMass* in this study) corrected by an attenuation factor corresponding to its size (Fleming, 1970) and by the moisture of the surrounding matrix (Zimmerman, 1971). The self-dose of the grain can also be considered, but it is only affected by the size of the grain; this self-dose is then the exact complement of that of the matrix (because of the principle of superposition) if the grain and the matrix are made of the same components. This configuration has been reproduced in *DosiVox* by modeling a single grain, surrounded by a matrix that is uniform in terms of chemical composition, density, moisture and radioactivity. The grain self-dose and the dose from the matrix were calculated for different radiations and configurations. The volume of the model has been adapted in each case in order to have in all directions a matrix whose dimensions are larger than the maximum range of the particles considered in the medium.

The results of the $\alpha$-dose rate simulation for the U- and Th-series spectra are shown in Fig. 7. The attenuation factors in a 100 $\mu$m diameter quartz grain for the self-dose and the dose from the matrix have been obtained by dividing the dose recorded in the grain by the *EmMass* values, respectively of the grain and the surrounding matrix. The grain is composed of $SiO_2$ with a density of 2.65 g cm$^{-3}$, which corresponds to quartz, and the matrix is also made of $SiO_2$ but with a density of 1.8 g cm$^{-3}$ in order to represent a siliceous sediment. The moisture is zero.

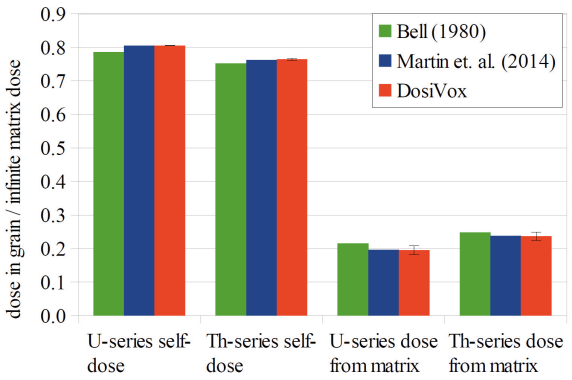


Figure 7. $\alpha$-dose attenuation in 100 $\mu$m diameter quartz grain.

The *DosiVox* results are compared to the data calculated by Bell (1980) and Martin et al. (2014) for $\alpha$-dose attenuation. The data from Martin et al. were obtained with a specific Geant4 code and are corrected for the matrix effect i.e. in taking into account the siliceous composition of the matrix. One can see on Fig. 7 that the *DosiVox* results match the data from Martin et al. and are close to Bell's calculations, what suggests a good reliability of the software for simulating $\alpha$-particles.

The $\beta$-dose rate attenuation factors for self-dose in 100 $\mu$m and 1 mm grains, as the dose from the matrix in the case of a 1 mm grain, are given in Fig. 8. The $\beta$-spectra available in *DosiVox* for $^{40}$K, U-series and Th-series have been used. The grains are composed of quartz, and both a silica matrix ($SiO_2$ 100 %) and a clay matrix ($SiO_2$ 54 %, $Al_2O_3$ 46 %), both with density 1.8 g cm$^{-3}$, have been considered. The results are compared to the data from Guérin et al. (2012) concerning the $\beta$-dose rate attenuation for various grain sizes, deduced from the self-dose in quartz grains. A good agreement is found between the Guérin and *DosiVox* results. Small differences can be observed but remain lower than 3 %. They could possibly be explained by different assumptions made in the simulation. For the *DosiVox* simulations performed with a 1 mm grain, one can observe a perfect complementarity of the self-dose and the dose in the case of the silica matrix in agreement with the principle of superposition. It is also noticeable that a non-negligible difference can be observed between the dose rate from the silica and the clay matrix. Similar observations were made by Martin et al. (2014) for the $\alpha$-dose rate in grains resulting in an attenuation factor depending on the matrix chemical composition. This effect on the $\beta$-dose rate could result in significant sys-

tematic errors in age calculation if not taken into account. In particular, it could be important for fine grains whose $\beta$-self-dose contribution is smaller than coarse grains, or for matrices whose chemical composition is significantly different from silica (since pure silica was the material usually used for calculating $\beta$-dose attenuation factors).

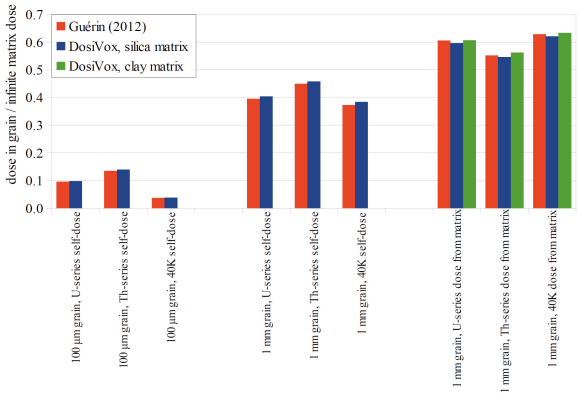


Figure 8. $\beta$-dose attenuation in 100 $\mu$m and 1 mm diameter quartz grains.

It is also well known that the sediment moisture content has a considerable impact on the attenuation of the dose rates because of the higher probability of interaction of the ionizing particles with water in comparison to the solid materials present in sediments (Aitken, 1985). Taking in account the effect of moisture on dose rates has a significant impact in dating. In order to assess this effect with *DosiVox*, different contents of water have been added to the previously used silica and clay matrices. The attenuated dose rates obtained are showed in Fig. 9.

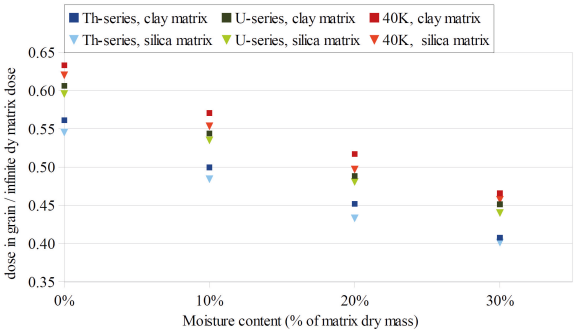


Figure 9. Impact of the matrix moisture content on the $\beta$-dose in 1 mm quartz grain.

Considering the equation of Zimmerman (1971) for taking into account the effect of water on the $\beta$-dose rate in a sediment, it is possible to use the results of these simulations to calculate the $\chi$-factor which represents the ratio of $\beta$-dose absorption between the water and the sediment. If an equal contribution of the $^{40}$K, Th- and U-series $\beta$-emissions is considered, values of $\chi = 1.20 \pm 0.02$ are calculated for the $\beta$-dose rate in both the silica and clay matrices. It is noticeable that, since these materials have different $\beta$-dose absorptions, they should lead to different $\chi$-values, as it was already noticed by Martin et al. (2014) about the effect of moisture on the $\alpha$-dose rate. But as one can observe on Fig. 9, this difference remains small for $\beta$-radiations. Moreover, the $\chi$-value obtained with the *DosiVox* simulations is consistent with the value of 1.19–1.20 calculated by Nathan & Mauz (2008) for carbonate-rich sediments (Notice that these authors used another Monte-Carlo code -MCNP- for their simulations). Finally, if the emission of the $^{40}$K is considered as the main contribution of the $\beta$-dose rate in the clay matrix, the $\chi$-value calculated by the *DosiVox* simulations is closer to 1.19.

## 4.2. Complementarity of external and internal $\beta$-dose rates

The modeling of a single grain embedded in an infinite homogeneous matrix is not representative of sediments presenting a relative high proportion of grains. Dosimetric effects can be induced by the presence of grains next to each other. A common way to model these effects is to create a random packing of spheres, representing the grains, in order to simulate the dose rate in this geometry (Guérin et al., 2012). *DosiVox* offers this possibility by including a grain-packing algorithm, each grain created being an independent detector recording the dose it receives during the simulation. It is difficult to have a point of comparison for this kind of results because of the lack of similar calculations. The modeling of Nathan et al. (2003), Brennan (2006) or Guérin et al. (2012) focused on polymineral grain packings, with different radioactive contents, a situation not possible to reproduce in *DosiVox*: only one grain composition can be defined in a packing, and the particle emission can originate either from the matrix or from the grains. We then propose to test a more basic assumption in order to contribute to the validation of this kind of modeling: the principle of superposition of the dose rate. According to this principle, if two different parts of the dose rate are calculated separately, the total dose rate should be the sum of the two calculated ones.

The modeling that we consider here is composed of a grid of $3 \times 3 \times 3$ cubic voxels of 5 mm in size each one (for a total grid size of $15 \times 15 \times 15$ mm), filled with silica ($SiO_2$, density: 2.65 g cm$^{-3}$). In the central voxel, 400 $\mu$m diameter silica grains, representing 30 % of the voxel volume (about one thousand grains), are separated from the surrounding matrix (Fig. 10). All the volume is homogeneous in terms of material and radioactivity. The $\beta$-particles emitted from the grains or from the surrounding matrix and the adjacent voxels are simulated separately. One considers here the $\beta$-spectrum of the Th-series only. The doses deposited in the grains, originating from the grains or from the surrounding environment respectively, were recorded and compared to the infinite matrix dose rate (corresponding respectively to the grain *EmMass* and to the matrix *EmMass*). The average dose deposited in the grains and originating from the grains corresponds to $37 \pm 1$ % of the infinite matrix dose rate. The average dose deposited in the grains, but originating from the surrounding environment, corresponds to $63 \pm 1$% of the infinite matrix dose rate. The sum of the two dose rates is

then compatible with 100, which fully satisfies the principle of superposition.

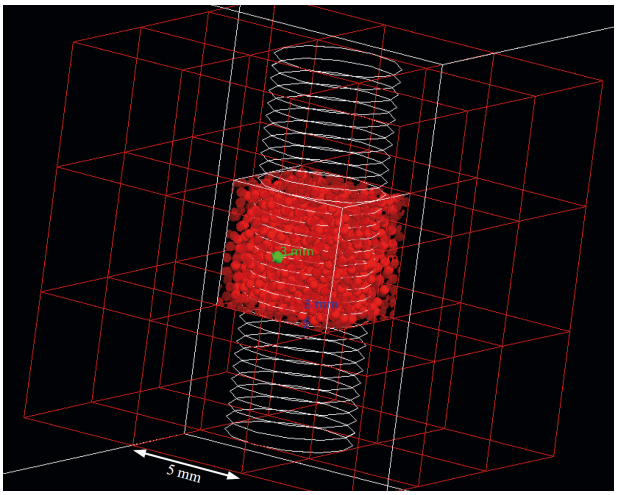


Figure 10. Visualization of the random packing of 400 $\mu$m grains for the $\beta$-dose rate complementarity test.

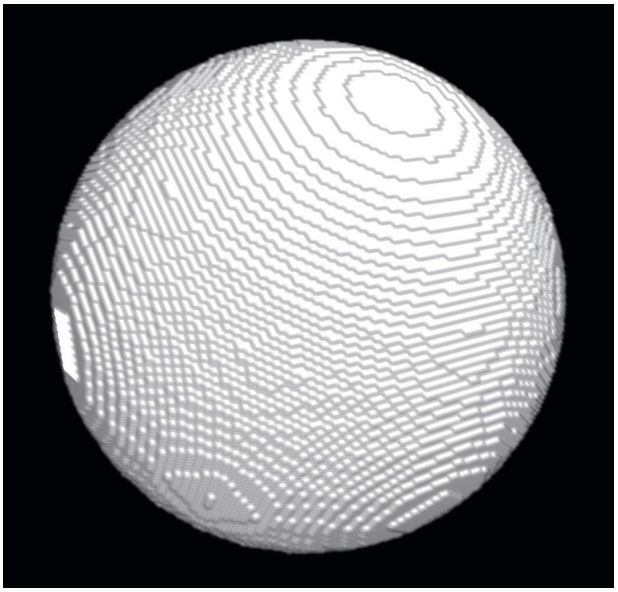

Figure 11. Voxelised modeling of a sphere.

## 5. Dose rate attenuation in a voxelised sphere

This last simulation layout purpose is to test the reliability of a voxelised modeling to represent an object for dose rate calculation. More precisely, the sub-voxelised detector of *DosiVox* was used to represent a 100 voxels diameter sphere. This modeling was constructed by loading a 3D image of a sphere in the *DosiVox* interface for the creation of a "pilot" text file (Martin et al., 2015a) (Fig. 11). As the size of the voxels can be changed, the total size of the sphere can be adjusted for different modelings. The results of the simulations of $\alpha$-, $\beta$- and $\gamma$-dose rates in spheres of various dimensions, and various materials in the case of the $\gamma$-emissions, are presented in Table 1 and compared to standard attenuation factors for these configurations.

The results of the dose rates simulated with *DosiVox* using the voxelised modeling of spheres are in good agreement with the reference data. However, a non-negligible bias can be observed for the $\gamma$-self-dose compared to the data from Aitken (1985), derived from Mejdahl (1983) and presented as approximations to evaluate the $\gamma$-dose rate in a sphere. These differences may result from the incomplete $\gamma$-spectrum used by Mejdahl or by the fact that Aitken approximated the data rather than using an exact equation. Moreover, the *DosiVox* simulations of the self-doses in a non-voxelised 10 cm sphere (i.e. in the same layout as for section 3 calculations) gave results identical to the simulations of the voxelised spheres within the range of 1 %. We can then conclude that voxelised modeling with reasonable resolution can be considered as representative of non-voxelised modeling.

In addition to the average self-dose rate in a sphere, the sub-voxelised detector of *DosiVox* creates a three-dimensional mapping of the dose deposited in the form of successive text files containing a matrix of dose values, each file representing the dose deposited in a slice of the model. It is possible to read this series of text files with an image processing software, like *ImageJ* (Rasband, 1997; Schneider et al., 2012), to visualize and study the dose in each slice, or to reconstruct the 3D-mapping of the dose deposited (Fig. 12). Using this process or the records of the "Probe" detector of *DosiVox*, one can obtain the dose profile through simulation (Fig. 13). The various dosimetric data collected by voxelised modeling in *DosiVox* could bring useful information for better understanding the dosimetric phenomena encountered in paleodosimetric dating.

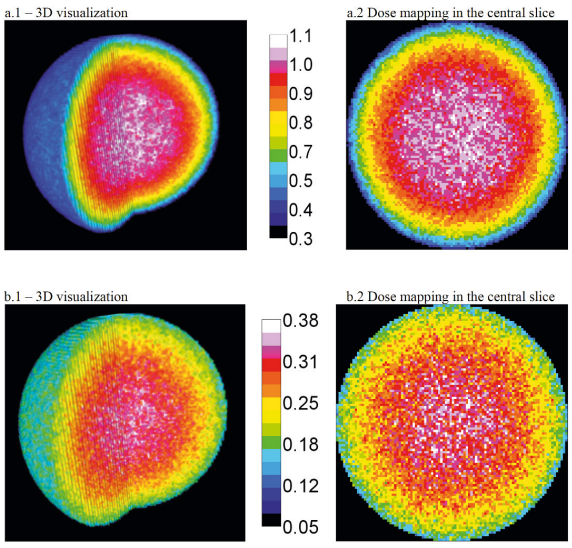


Figure 12. Self-dose mapping in voxelised spheres.

| Radiation (Series) | Diameter of the sphere | Density (g cm$^{-3}$) | Material | *DosiVox* (Selfdose/*EmMass*) | Reference value | Reference publication | Difference |
|---|---|---|---|---|---|---|---|
| $\alpha$ (Th) | 100 $\mu$m | 2.65 | Silica | 0.765 | 0.764 | Martin et al. (2014) | 0.02 % |
| $\beta$ (Th) | 100 $\mu$m | 2.65 | Silica | 0.136 | 0.134 | Guérin et al. (2012) | -1.57 % |
| $\beta$ (Th) | 1 mm | 2.65 | Silica | 0.455 | 0.449 | Guérin et al. (2012) | -1.30 % |
| $\gamma$ (Th) | 10 cm | 2.65 | Silica | 0.242 | 0.265 | Aitken (1985) | 9.46 % |
| $\gamma$ (Th) | 10 cm | 2 | Clay | 0.186 | 0.200 | Aitken (1985) | 7.43 % |

Table 1. : $\alpha$-, $\beta$- and $\gamma$-self-doses in the voxelised modeling of a sphere.

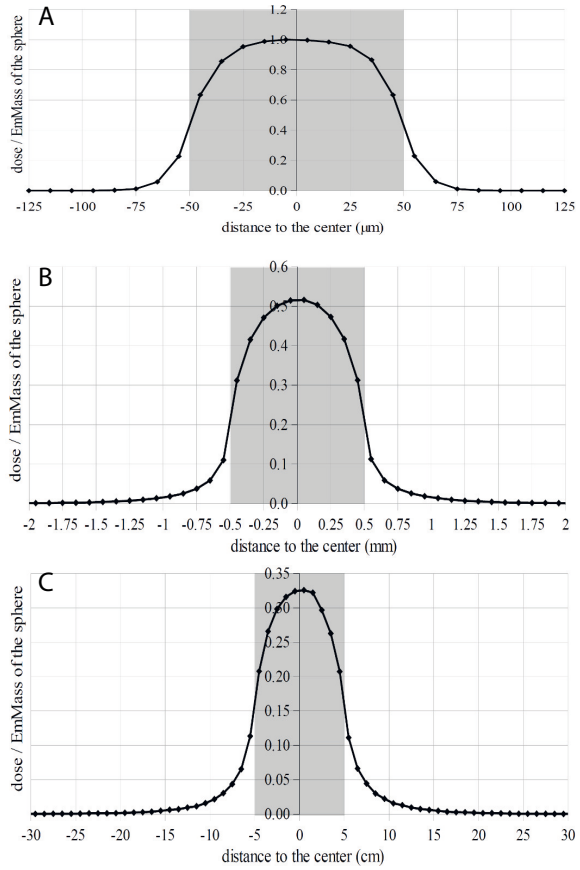


Figure 13. Dose rate profiles along the middle axis of voxelised radioactive spheres.

## 6. Conclusion

The results of the *DosiVox* simulations for the cases presented here are consistent with the already published data. Some differences can be observed but may be due to nuclear and cross sections data updates, or to small differences between the modelings in *DosiVox* and the previous representations. More important is the fact that the principle of superposition has been successfully tested in different modeling cases. Moreover, *DosiVox* offers tools allowing accessing spatially detailed information about the dose rates, in clusters of grains, or through three-dimensional dose rate mapping.

In addition to the comparison with usual data, the *DosiVox* results highlight the limits of some assumption frequently used: the $\gamma$-dose rate close to the surface of a sediment does not perfectly match the half of the infinite matrix dose rate in real environment conditions. We also observed that a non-negligible difference is observed between the attenuation of the matrix $\beta$-dose in grain and the usual way to calculate it by taking the complement of the self-dose factor of the grain. This observation had already been made by Martin et al. (2014) about the effects of the matrix composition on the $\alpha$-dose rate in grains. These observations demonstrate that, since it is impossible to gather dosimetric data about all the possible cases to be encountered in paleodosimetric dating, Monte-Carlo simulations are of great help for dose rate investigations. *DosiVox*, by its accessibility, could bring easy solutions for dose rate calculations in the cases exceeding the infinite matrix hypothesis.

Comparisons with the tabulated data, often obtained by numerical calculations and Monte-Carlo simulations, is only a first step for testing the reliability of *DosiVox*. The various possibilities of modeling available exceed the dosimetric layout documented in the literature. A most pertinent validation would be to compare the results of *DosiVox* obtained in complex dosimetric cases with experimental measurements. However, this way is difficult to implement because of the need to use detectors for dose measurements, which could represent a bias compared to a modeling and add a necessary step of calibration with a potential uncertainty when calculating doses. A special care has to be taken to achieve both experimental measurements and corresponding modeling but these comparisons need undoubtly to be done.

## Acknowledgments

The authors are grateful to the Aquitaine Region Council for funding this research through the program: DOSI-ART - DOSe reconstruction In archaeological ARTefacts and sediments. This work was also supported by the French National Research Agency via the LaScArBx Labex (project number ANR-10-LABX-52).

## References

Aitken, M J. *Thermoluminescence dating*. Studies in archaeological science. Academic Press, 1985. ISBN 9780120463817.

Bell, W T. *Alpha dose attenuation in quartz grain for thermoluminescence dating*. Ancient TL, 12(1): 1–5, 1980.

Brennan, B J. *Variation of the alpha dose rate to grains in heterogeneous sediments*. Radiation Measurements, 41: 1026–1031, 2006.

Brennan, B J, Rink, W J, McGuirl, E L, Schwarcz, H P, and Prestwich, W V. *Beta doses in tooth enamel by "one-group" theory and the ROSY ESR dating software*. Radiation Measurements, 27 (2): 307–314, 1997. doi: 10.1016/S1350-4487(96)00132-1.

Cross, W G, Freedman, N O, and Wong, P Y. *Tables of beta-ray dose distributions in water*. Technical Report AECL-10521, Chalk River Laboratoris, Chalk River, Onario, 1992.

Fain, J, Soumana, S, Montret, M, Miallier, D, Pilleyre, T, and Sanzelle, S. *Luminescence and ESR dating Beta-dose attenuation for various grain shapes calculated by a Monte-Carlo method*. Quaternary Science Reviews, 18(2): 231–234, 1999. doi: 10.1016/S0277-3791(98)00056-0.

Fleming, S J. *Thermoluminescent dating: refinement of the quartz inclusion method*. Archaeometry, 12(2): 133–143, 1970.

Grün, R. *Beta attenuation in thin layers*. Ancient TL, 4: 1–8, 1986.

Grün, R. *Alpha dose attenuation in thin layers*. Ancient TL, 5: 6–8, 1987.

Guérin, G, Mercier, N, Nathan, R, Adamiec, G, and Lefrais, Y. *On the use of the infinite matrix assumption and associated concepts: A critical review*. Radiation Measurements, 47(9): 778–785, 2012. doi: 10.1016/j.radmeas.2012.04.004.

Martin, L, Mercier, N, and Incerti, S. *Geant4 simulations for sedimentary grains in infinite matrix conditions: The case of alpha dosimetry*. Radiation Measurements, 70: 39–47, 2014. doi: 10.1016/j.radmeas.2014.09.003.

Martin, L, Incerti, S, and Mercier, N. *DosiVox: Implementing Geant 4-based software for dosimetry simulations relevant to luminescence and ESR dating techniques*. Ancient TL, 33(1): 1–10, 2015a.

Martin, L, Mercier, N, Incerti, S, Lefrais, Y, Pecheyran, C, Guérin, G, Jarry, M, Bruxelles, L, Bon, F, and Pallier, C. *Dosimetric study of sediments at the beta dose rate scale: Characterization and modelization with the DosiVox software*. Radiation Measurements, 81: 134–141, 2015b. doi: 10.1016/j.radmeas.2015.02.008.

Mejdahl, V. *Thermoluminescence dating: beta-dose attenuation in quartz grains*. Archaeometry, 21: 61–72, 1979.

Mejdahl, V. *Feldspar inclusion dating of ceramics and burnt stones*. PACT, 9: 351–364, 1983.

Nathan, R P and Mauz, B. *On the dose-rate estimate of carbonate-rich sediments for trapped charge dating*. Radiation Measurements, 43(1): 14–25, 2008. doi: 10.1016/j.radmeas.2007.12.012.

Nathan, R P, Thomas, P J, Jain, M, Murray, A S, and Rhodes, E J. *Environmental dose rate heterogeneity of beta radiation and its implications for luminescence dating: Monte Carlo modelling and experimental validation*. Radiation Measurements, 37(4-5): 305–313, 2003. doi: 10.1016/S1350-4487(03)00008-8.

Rasband, W S. *ImageJ, U.S. National Institutes of Health, Bethesda, Maryland, USA*. Technical report, 1997. URL http://imagej.nih.gov/ij/.

Schneider, C A, Rasband, W S, and Eliceiri, K W. *NIH Image to ImageJ: 25 years of image analysis*. Nature Methods, 9(7): 671–675, 2012. doi: 10.1038/nmeth.2089.

Zimmerman, D W. *Thermoluminescent dating using fine grains from pottery.* Archaeometry, 13(1): 29–52, 1971. doi: 10.1111/j.1475-4754.1971.tb00028.x.

## Reviewer

Nigel Spooner